2011

Transformation optics and metamaterials

A. V. Kildishev
Birck Nanotechnology Center, Purdue University, kildishev@purdue.edu

V. M. Shalaev
Birck Nanotechnology Center and School of Electrical and Computer Engineering, Purdue University, shalaev@purdue.edu

REVIEWS OF TOPICAL PROBLEMS

CELEBRATING 50 YEARS OF THE LASER

Transformation optics and metamaterials

A V Kildishev, V M Shalaev

Contents

Abstract. We review recent progress in developing a new class of specially designed optical metamaterial spaces with functionalities that cannot be obtained with conventional optics or natural materials. These optical metamaterial spaces could enable innovative paradigms of transformation optics pertinent to optical cloaking, sub-wavelength sensing, super-resolution imaging, magnifying hyperlenses, and light-concentrating devices. We also outline our recent development and deployment of an easy-to-use, multifaceted, on-line research environment for the nanophotonics research community. In particular, we show representative examples of two online software tools addressing a growing need for efficient numerical simulations in the area of transformation optics.

1. Introduction

Metamaterials (MMs) are rationally designed, artificial materials with versatile properties that can be tailored to fit a given practical need, and often go well beyond what can be obtained with 'natural' materials (see, e.g., [1, 2]). Recent progress in developing optical MMs by several leading groups has allowed unprecedented control over the flow of light on both the nano- and macroscopic scales. The innovative field of transformation optics (TO), which is enabled by metamaterials, is inspiring researchers to take a fresh look at the very foundations of optics and create a new paradigm for the

science of light [3, 4]. Similarly to general relativity, where time and space are curved, transformation optics shows that the space for light can also be bent in an almost arbitrary way. Most importantly, the optical space can be designed and engineered, opening the fascinating possibility of controlling light flow with nanometer spatial precision [5]. Far-fetched as it may appear, general relativity can actually be put to practical use in a number of novel optical devices based on transformation optics, guiding how the space for light can be curved in a pre-designed and well-controlled way using metamaterials.

This paper aims to review the recent progress in developing a new class of specially designed optical materials and devices with functionalities not obtainable with conventional optics and natural materials. This review addresses methods for overcoming the existing limitations of standard optical and optoelectronic devices by developing 3D optical MMs designed to control the flow of light on both the nano- and macroscopic scales with extreme precision and providing new, advanced functionalities. These extreme MMs incorporate the innovative theories of transformation optics and are pertinent to the important areas of optical cloaking, sub-wavelength sensing, super-resolution imaging, magnifying hyperlenses, and light-concentrating devices. One of the most exciting applications of the TO concept is an electromagnetic cloak that can bend light around itself, similarly to the flow of water around a stone in a stream, making both the cloak and any object hidden inside it invisible [3, 6–9].

Here, we focus on another important application — a flat hyperlens that can magnify small, nanometer-scale features of an object that cannot be resolved with conventional optics [10]. By enabling nanoscale resolution in optical microscopy, metamaterial-based transformation optics could allow the visualization of extremely small objects such as biological cells, viruses, and possibly even DNA molecules. This can revolutionize the field of optical imaging simply by including a meta-lens as a standard add-on tool for microscopes.

A V Kildishev, V M Shalaev Birck Nanotechnology Center School of Electrical and Computer Engineering, Purdue University, 1205 W State Street, West Lafayette, IN 47907-2057 USA, Tel. + 1 (765) 496-3196, + 1 (765) 494-9855. Fax + 1 (765) 496-6443 E-mail: kildishev@purdue.edu, shalaev@purdue.edu

A different TO application example is a nonimaging light-concentrating device, which is conceptually similar to the hyperlens and can be used for efficient solar light collection in photovoltaic elements for renewable energy [10, 11].

An important component of the paper is an overview of our broader impact and outreach activities through education and knowledge transfer by using the cyber-infrastructure available at nanHUB.org and the Network for Computational Nanotechnology.

2. Transformation optics

Transformation optics (TO) is a new paradigm for the science of light that is enabled by recent developments in metamaterials. In accordance with the Fermat principle, light propagates such that the optical path is minimized, i.e., $\int_A^{A'} n(\mathbf{r}) \, \mathrm{d}r$ is stationary with respect to the AA' path variations. Hence, by creating a complex distribution of refractive indices $n(\mathbf{r})$, the *geometrical* path of light that minimizes the *optical* path can be curved in a desired fashion. In semiclassical transformation optics (SCTO), a distribution of refractive indices $n(\mathbf{r})$ is designed that allows light waves to propagate not only in the backward direction [when $n(\mathbf{r})$ is negative], but also along curved lines. Although SCTO methods work in general within the limitations of geometrical optics, in many cases only metamaterials can provide the desired distribution of the effective refractive index.

The theoretical foundation of full-wave transformation optics (FWTO) is built on the invariance of Maxwell's equations under coordinate transformations, provided that the basic optical parameters of materials — the dielectric permittivity $\varepsilon(\mathbf{r})$ and magnetic permeability $\mu(\mathbf{r})$ tensors — are also transformed appropriately. This allows molding and controlling light on all scales, from the macroscopic down to the deeply sub-wavelength ones. The most comprehensive and extreme control of electromagnetic energy flow can be achieved by creating a desired distribution of $\varepsilon(\mathbf{r})$ and $\mu(\mathbf{r})$ or using the full-wave transformation-optics approach, as we call it here, such that the space for light can be 'curved' in a nearly arbitrary way [3–7, 10, 12–20]. For example, by excluding light from a certain area of space and bending light around the region, similarly to how water flows around a stone in a stream, an object in that area can be made to appear invisible or 'cloaked.' A kind of 'anti-cloak' that concentrates light within a certain area can also be created by collecting light from all directions into an arbitrarily small spot [10]. Finally, a flat magnifying hyperlens could be developed, which could revolutionize the imaging of objects with light because it could be used as a standard add-on tool for conventional microscopes and provide nanoscale spatial resolution [21].

In this section, we introduce equations that describe the mathematical apparatus of the TO approach. The mathematical foundations described here are needed for understanding the key principles of creating metamaterial spaces for light.

2.1 FWTO: vectors, matrices, and Maxwell's equations
A general curvilinear transformation $\mathbf{r} = \mathbf{r}(\tilde{\mathbf{r}})$ connects the points in a virtual coordinate system $\tilde{\mathbf{r}} = (v, \tau, \eta)$ with the points of the physical world $\mathbf{r} = (z, y, z)$. A triplet of arbitrary noncoplanar base vectors $\mathbf{e}_q = \partial\mathbf{r}/\partial q = \mathbf{r}^{(q)}$, with $q = v, \tau, \eta$, naturally defines the coordinate unit vectors $\hat{\mathbf{e}}_q = \mathbf{e}_q|\mathbf{e}_q|^{-1}$ projected from the virtual space. The basic vector identities (see, e.g., [22], p. 27) $\mathbf{v} = \sum v^q \mathbf{e}_q$ and $\mathbf{v} = \sum v_q \mathbf{e}^q$ hold for any

noncoplanar vectors, $\mathbf{e}_v \mathbf{e}_\tau \mathbf{e}_\eta \neq 0$, where $v_q = \mathbf{e}_q \mathbf{v}$ and $v^q = \mathbf{e}^q \mathbf{v}$, with $q = v, \tau, \eta$. The vector $\tilde{\mathbf{v}}$ is defined as $\tilde{\mathbf{v}} = \mathbf{j}^T \mathbf{v}$, where $\mathbf{j}^T$ is the transposition of the Jacobian matrix $\mathbf{j}$; the matrix $\mathbf{j}$ and the vector $\tilde{\mathbf{v}}$ are constructed from the base vectors and the scalar components as $\mathbf{j} = (\mathbf{e}_v \; \mathbf{e}_\tau \; \mathbf{e}_\eta)$ and $\tilde{\mathbf{v}} = (v_v \; v_\tau \; v_\eta)^T$. From $\mathbf{v} = \mathbf{j} \mathbf{v}^0$, it also follows that $\mathbf{v}^0 = \mathbf{j}^{-1} \mathbf{v}$, where $\mathbf{v}^0 = (v^v \; v^\tau \; v^\eta)^T$. Because the determinant $|\mathbf{j}|$ is equal to $\mathbf{e}_v \mathbf{e}_\tau \mathbf{e}_\eta$ [22], the reciprocal vectors are given by $\mathbf{e}^v = |\mathbf{j}|^{-1} \mathbf{e}_\tau \times \mathbf{e}_\eta$, $\mathbf{e}^\tau = |\mathbf{j}|^{-1} \mathbf{e}_\eta \times \mathbf{e}_v$, and $\mathbf{e}^\eta = |\mathbf{j}|^{-1} \mathbf{e}_v \times \mathbf{e}_\tau$; we note that $\mathbf{e}_p \mathbf{e}^q = \delta_p^q$, with δ_p^q being the Kronecker delta.

The curl of a given vector $\mathbf{v}$ in a general curvilinear coordinate system can be derived from its definition

$$\mathbf{n} \cdot \mathrm{curl}\, \mathbf{v} = \lim_{\Omega \to 0} \frac{1}{\Omega} \oint_C \mathbf{v} \cdot \mathrm{d}\mathbf{r},$$

where a contour C bounds a small area Ω, and $\mathbf{n}$ is the unit normal vector to Ω. Therefore,

$$
\begin{aligned}
\mathrm{curl}\, \mathbf{v} = |\mathbf{j}|^{-1} \big[& (v_\eta^{(\tau)} - v_\tau^{(\eta)})\mathbf{e}_v + (v_v^{(\eta)} - v_\eta^{(v)})\mathbf{e}_\tau \\
& + (v_\tau^{(v)} - v_v^{(\tau)})\mathbf{e}_\eta \big].
\end{aligned}
\tag{1}
$$

2.2 Invariance identity for Maxwell's equations
Now, to come closer to the Maxwell curl equations, yet another product of a tensor $\mathbf{m}$ and a vector $\mathbf{u}$ can be defined as $\mathbf{mu} = \mathrm{rot}\, \mathbf{v}$, and then it could be converted into new components by multiplying the vectors on both sides by $\mathbf{j}^{-1}$; this yields $\mathbf{j}^{-1} \mathbf{mu} = \mathbf{j}^{-1} \mathrm{rot}\, \mathbf{v}$.

The use of identical sets of vector components gives the invariance identity $|\mathbf{j}|\mathbf{j}^{-1}\mathbf{m}(\mathbf{j}^T)^{-1}\tilde{\mathbf{u}} = \tilde{\boldsymbol{\nabla}} \times \tilde{\mathbf{v}}$. It is crucial that $\tilde{\boldsymbol{\nabla}} \times \mathbf{v}$ now matches the standard curl in an orthogonal basis with unit vectors $\hat{\mathbf{v}}, \hat{\boldsymbol{\tau}}, \hat{\boldsymbol{\eta}}$, and $\hat{\mathbf{v}} = \hat{\boldsymbol{\tau}} \times \hat{\boldsymbol{\eta}}$, i.e.,

$$\tilde{\boldsymbol{\nabla}} \times \tilde{\mathbf{v}} = \begin{vmatrix} \hat{\mathbf{v}} & \hat{\boldsymbol{\tau}} & \hat{\boldsymbol{\eta}} \\ \partial_v & \partial_\tau & \partial_\eta \\ v_v & v_\tau & v_\eta \end{vmatrix}. \tag{2}$$

Finally, with $\tilde{\mathbf{m}} = |\mathbf{j}|\mathbf{j}^{-1}\mathbf{m}(\mathbf{j}^T)^{-1}$, the invariance identity can be written as $\tilde{\mathbf{m}}\tilde{\mathbf{u}} = \tilde{\boldsymbol{\nabla}} \times \tilde{\mathbf{v}}$, and the Maxwell curl equations $\boldsymbol{\nabla} \times \mathbf{E} = -\mu \mathbf{H}^{(t)}$ and $\boldsymbol{\nabla} \times \mathbf{H} = \varepsilon \mathbf{E}^{(t)}$ can be rewritten as a new set of similar equations, $\tilde{\boldsymbol{\nabla}} \times \tilde{\mathbf{E}} = -\tilde{\mu}\tilde{\mathbf{H}}^{(t)}$ and $\tilde{\boldsymbol{\nabla}} \times \tilde{\mathbf{H}} = \tilde{\varepsilon}\tilde{\mathbf{E}}^{(t)}$, where $\mathbf{H} = (\mathbf{j}^T)^{-1}\tilde{\mathbf{H}}$, $\mathbf{E} = (\mathbf{j}^T)^{-1}\tilde{\mathbf{E}}$, and

$$
\begin{aligned}
\varepsilon &= |\mathbf{j}|^{-1}\mathbf{j}\tilde{\varepsilon}\mathbf{j}^T, \\
\mu &= |\mathbf{j}|^{-1}\mathbf{j}\tilde{\mu}\mathbf{j}^T.
\end{aligned}
\tag{3}
$$

Hence, if the electromagnetic properties of the physical (material) space follow Eqns (3), then the Umov–Poynting vector $\mathbf{S} = (1/2)(\mathbf{E} \times \mathbf{H}^*)$ in the material world, given by

$$\mathbf{S} = |\mathbf{j}|^{-1}\mathbf{j}\tilde{\mathbf{S}}, \tag{4}$$

follows the behavior of the Umov–Poynting vector $\tilde{\mathbf{S}} = (1/2)(\tilde{\mathbf{E}} \times \tilde{\mathbf{H}}^*)$ in the virtual space.

Transformations (3) and (4) solve a fundamental problem of designing a continuous material space for a desired spatial transformation of electromagnetic vectors and therefore the problem of achieving a required functionality. In other words, for the physical Umov–Poynting vector $\mathbf{S}$ to match the corresponding distribution of the virtual Umov–Poynting vector $\tilde{\mathbf{S}}$, the material properties should obey Eqns (3).

2.3 Superlens

We suppose, for example, that the emulation of the electromagnetic fields in left-handed coordinates $(-\hat{\mathbf{v}} = \hat{\boldsymbol{\tau}} \times \hat{\boldsymbol{\eta}}, -\hat{\boldsymbol{\tau}} = \hat{\boldsymbol{\eta}} \times \hat{\mathbf{v}}, -\hat{\boldsymbol{\eta}} = \hat{\mathbf{v}} \times \hat{\boldsymbol{\tau}})$ is desired in a metamaterial space beyond a planar boundary Γ. This would suggest that physical points beyond Γ are projected from the virtual points using a mirror symmetry relative to Γ, i.e., $x = -v$, $y = \tau$, and $z = \eta$. As a result, $\mathbf{j} = \mathrm{diag}\,(-1, 1, 1)$, and the required material space beyond Γ should match the ideal, isotropic, double-negative material of the Veselago–Pendry lens [3, 23–28], i.e., $\mu = \varepsilon = -\mathbf{i}$ ($\mathbf{i}$ is the identity matrix). In accordance with $\mathbf{v} = (\mathbf{j}^{\mathrm{T}})^{-1}\tilde{\mathbf{v}}$, where $\mathbf{v}$ is $\mathbf{E}$, $\mathbf{H}$, or $\mathbf{k}$, the component of the vector field along the direction of the normal to Γ is reversed ($v_x = -\tilde{v}_v$), while the other two components remain intact ($v_y = \tilde{v}_\tau$, $v_z = \tilde{v}_\eta$). In contrast to the field vectors, the components of the pseudovectors $\mathbf{S} = |\mathbf{j}|^{-1}\mathbf{j}\tilde{\mathbf{S}}$ demonstrate the opposite behavior, $S_x = \tilde{S}_v$, $S_y = -\tilde{S}_\tau$, and $S_z = -\tilde{S}_\eta$, thus supporting negative refraction of arbitrarily polarized light. The dispersion relation in the virtual left-handed space $(\tilde{k}_v^2 + \tilde{k}_\tau^2 + \tilde{k}_\eta^2 - \tilde{k}_0^2 = 0)$ is identical to that in the metamaterial space, $-(k_v^2 + k_\tau^2 + k_\eta^2) + k_0^2 = 0$, and therefore light propagates in this metamaterial as if it were propagating in a left-handed space [29].

2.4 Planar hyperlens

The translation properties of the Veselago–Pendry lens are related to its thickness [3, 23, 24, 30, 31], and therefore a desired step would be to stretch the double-negative slab $(\tilde{\mu} = \tilde{\varepsilon} = -\mathbf{i})$ along the propagation direction and obtain a larger translation. For a scaling transformation $x = x(v)$, the modification of the metamaterial properties would require anisotropy, i.e., $\varepsilon = \mu = -\mathrm{diag}\,(x', x'^{-1}, x'^{-1})$, where $x' = x^{(v)}$. Unfortunately, the 'stretched' superlens is still a device with esoteric, double-negative, anisotropic properties, prone to losses and dispersion-engineering difficulties.

On top of the most important feature of the superlens, i.e., translation of the evanescent modes, additional magnification can be achieved by stretching the ordinary homogeneous space in the vicinity of near-field sources [10, 17, 19, 32–35].

We now consider a simplified 2D example where an almost hand-drawn family of light transfer traces is taken to describe the functionality of a given TO device — addressing, for example, a design of a magnifying, flat superlens. A set of such traces can be defined by an initial generating line $y_i = f(x)$, scaled in the physical space using a morphing function $s(\tau)$, such that

$$y(x, \tau) = s(\tau) f(x)\,. \tag{5}$$

In general, the family of generating lines defined by Eqn (5) can be regarded as a set of coordinate lines of an appropriate orthogonal coordinate system (v, τ), as shown in Fig. 1a. The generating lines project the input light at $x = 0$ (for example, point A) onto the output boundary at the other side of the lens $x = x_0$ (at point A''), as shown in Fig. 1b. It would be desirable to avoid aberrations, and hence the simplest linear transformation is taken:

$$s(\tau) = \tau = \frac{y}{f(x)}\,. \tag{6}$$

Then the set of orthogonal coordinate lines $x = x(v, y)$, $v = \mathrm{const}$ is obtained using the fundamental identity of an
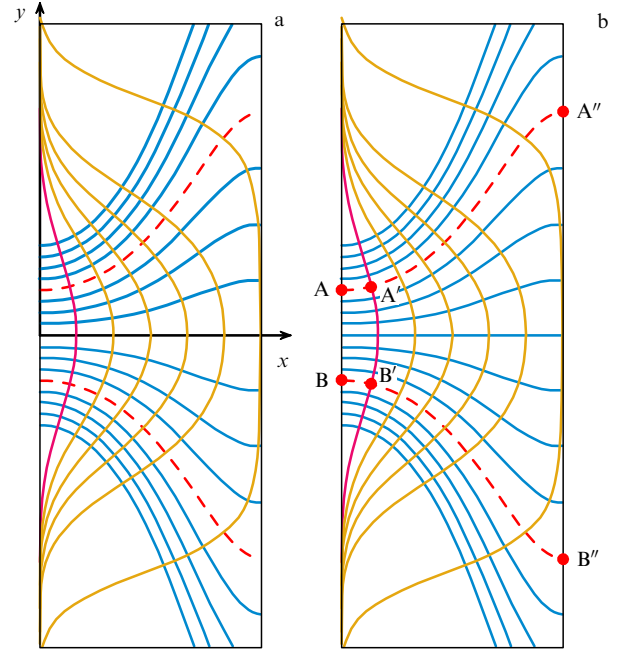

Figure 1. (a) Generating lines (red) and the matching orthogonal curvilinear coordinates. (b) Mapping the near-field virtual domain AA′B′B onto a material domain AA″B″B (with a scaling transformation).

orthogonal coordinate system,

$$\frac{\mathrm{d}x}{\mathrm{d}y} = -\tau f' = -y \ln' f\,, \tag{7}$$

where f' and $\ln'$ denote the derivatives of $f(x)$ and $\ln(x)$ with respect to x (the argument is omitted for brevity). Solving separable differential equation (7), we finally obtain

$$\int \frac{\mathrm{d}x}{\ln' f} + \frac{1}{2}\, y^2 + C = 0\,. \tag{8}$$

To illustrate this approach, we take $f = \exp\,(ax^3 + bx^2 + d)$ as an example, with the logarithmic derivative $\ln' f = 3ax^2 + 2bx$. After choosing the design parameters of the lens, i.e., magnification (m), thickness (l), and the scale of the lens geometry at $\tau = 1$ $(y_0 = \exp d)$, we restrict the traces further by forcing them to become orthogonal to the output boundary of the slab, while still providing the required magnification. Therefore, we write

$$\begin{cases} f'(l) = 0 \\ f(l) = my_0 \end{cases}\,. \tag{9}$$

Solving system (9), we then obtain the parameters of the generating lines, $a = -2l^{-3}\ln m$ and $b = 3l^{-2}\ln m$, and from (8) we subsequently obtain the orthogonal coordinate lines

$$x(x_i, y) = \frac{2bx_i}{\exp\,(by^2)\,(3ax_i + 2b) - 3ax_i}\,, \tag{10}$$

where the constant in Eqn (8) is defined by $C = \ln\,(3a + 2b/x_i)/(2b)$, with x_i being the position on the x axis at $y = 0$.

The corresponding orthogonal map is shown in Fig. 1b. Once the desired orthogonal coordinate line system is known, the design of the material space for light becomes trivial and follows general recipes, for example, those discussed in [3, 10, 15, 17].

In essence, the mapping transformation of the virtual space AA′B′B onto the material space AA″B″B defines the
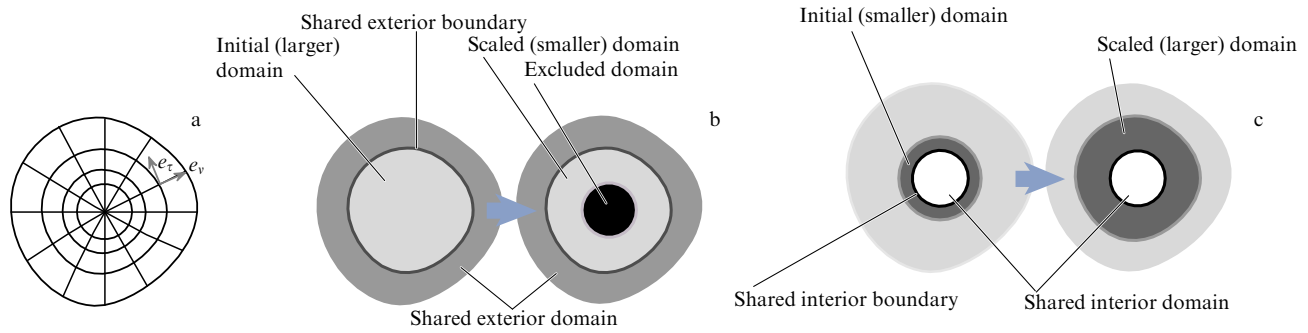
Figure 2. (a) Example of a general orthogonal cylindrical coordinate system. (b) Domain transformation for a cylindrical cloaking device. The larger initial (pink) domain in the left panel is mapped onto the scaled smaller annular domain shown in the right panel, leaving the central (black) domain inaccessible to light. The initial and scaled domains share the same exterior boundary and the common space beyond. (c) Domain transformation for a hyperlens. The smaller initial domain in the left panel is mapped onto the scaled larger domain in the right panel. The initial and scaled domains share the same internal boundary and a common space inside it.

anisotropic metamaterial space of a flat magnifying hyperlens, because any evanescent wave with nonzero magnitude at segment $A'B'$ in the virtual free-space without the lens is to be seen through the anisotropic metamaterial lens at segment $A''B''$. Hence, the evanescent modes are both translated and magnified. This approach could modernize the conventional imaging of objects with light by providing easily obtainable nanoscale spatial resolution.

We note that as the distance between AA' and BB' decreases, i.e., the initial virtual space for light becomes more confined, and the required metamaterial parameters become more extreme. We also note that the orthogonal curvilinear coordinate system in Fig. 1a belongs to the class of *general orthogonal cylindrical coordinate systems* that are arranged by translating a map of $x-y$ coordinate lines perpendicular to the $x-y$ plane. In this case, for any coordinate transformation exploiting a *scaling transformation* along a single coordinate, e.g., using a v-scaling of segments AA' and BB' onto AA'' and BB'' as shown in Figs 1a, b, the complexity of TO problems in TE or TM formulations is significantly reduced.

2.5 Scaling transformations

If a 2D radius vector is defined by a parametric vector function $\tilde{\mathbf{r}}(\tilde{v}, \tilde{\tau})$ and a 2D field vector $\tilde{\mathbf{v}}$ is defined as $\tilde{\mathbf{v}} = \tilde{v}_{\tilde{v}}\hat{\mathbf{e}}_{\tilde{v}} + \tilde{v}_{\tilde{\tau}}\hat{\mathbf{e}}_{\tilde{\tau}}$, then the Jacobian matrix is the diagonal matrix $\tilde{\mathbf{s}} = \mathrm{diag}\,(s_{\tilde{v}}, s_{\tilde{\tau}})$, with the metric coefficients given by $s_{\tilde{v}} = [\tilde{\mathbf{r}}^{(\tilde{v})} \tilde{\mathbf{r}}^{(\tilde{v})}]^{1/2}$ and $s_{\tilde{\tau}} = [\tilde{\mathbf{r}}^{(\tilde{\tau})} \tilde{\mathbf{r}}^{(\tilde{\tau})}]^{1/2}$. With $y^{(x)}$ used to denote $\partial y/\partial x$, the following scalar wave equation holds [8]:

$$\left(\tilde{s}_{\tilde{\tau}}\tilde{m}_{\tilde{\tau}}^{-1}\tilde{s}_{\tilde{v}}^{-1}\tilde{v}^{(\tilde{v})}\right)^{(\tilde{v})} + \left(\tilde{s}_{\tilde{v}}\tilde{m}_{\tilde{v}}^{-1}\tilde{s}_{\tilde{\tau}}^{-1}\tilde{v}^{(\tilde{\tau})}\right)^{(\tilde{\tau})} - \omega^2 \tilde{m}_{\tilde{z}}|\mathbf{s}|v = 0\,. \quad (11)$$

Here, $\tilde{m}_{\tilde{v}}$ and $\tilde{m}_{\tilde{\tau}}$ are the only components of a diagonal material property tensor, i.e., anisotropic permeability or anisotropic permittivity (for TM or TE polarization, respectively). The scalar $\tilde{v}$ is the only component of the transverse field, i.e., the magnetic field $\mathbf{H} = \hat{\mathbf{e}}_z H_z$ (TM) or the electric field $\mathbf{E} = \hat{\mathbf{e}}_z E_z$ (TE). Similarly to (11), yet another wave equation in a new physical coordinate system (v, τ, z) is written as

$$\left(s_{\tau}m_{\tau}^{-1}s_{v}^{-1}v^{(v)}\right)^{(v)} + \left(s_{v}m_{v}^{-1}s_{\tau}^{-1}v^{(\tau)}\right)^{(\tau)} - \omega^2 m_z|\mathbf{s}|v = 0\,. \quad (12)$$

To mimic the behavior of light waves obeying (11), a scaling transformation $v = v(\tilde{v})$ [with $\tau = \tilde{\tau}$, $z = \tilde{z}$, and $v' = v^{(\tilde{v})}$] is introduced. To maintain similarity with (11), we bring

Eqn (12) to the form

$$\left(\left[\frac{1}{v'}\frac{s_{\tau}\tilde{m}_{\tilde{\tau}}\tilde{s}_{\tilde{v}}}{\tilde{s}_{\tilde{\tau}}m_{\tau}s_{v}}\right]\frac{\tilde{s}_{\tilde{\tau}}}{\tilde{m}_{\tilde{\tau}}\tilde{s}_{\tilde{v}}}v^{(\tilde{v})}\right)^{(\tilde{v})} + \left(\left[v'\frac{s_{v}\tilde{m}_{\tilde{v}}\tilde{s}_{\tilde{\tau}}}{\tilde{s}_{\tilde{v}}m_{v}s_{\tau}}\right]\frac{\tilde{s}_{\tilde{v}}}{\tilde{m}_{\tilde{v}}\tilde{s}_{\tilde{\tau}}}v^{(\tilde{\tau})}\right)^{(\tilde{\tau})}$$

$$- \omega^2 \left[v'\frac{m_z|\mathbf{s}|}{\tilde{m}_{\tilde{z}}|\tilde{\mathbf{s}}|}\right]\tilde{m}_{\tilde{z}}|\tilde{\mathbf{s}}|v = 0\,. \quad (13)$$

We see that (11) is completely identical to (13) if the ratios in the square brackets are each unity. It is therefore required that the TO identities

$$v'\frac{s_{v}\tilde{m}_{\tilde{v}}\tilde{s}_{\tilde{\tau}}}{\tilde{s}_{\tilde{v}}m_{v}s_{\tau}} = 1\,, \qquad \frac{1}{v'}\frac{s_{\tau}\tilde{m}_{\tilde{\tau}}\tilde{s}_{\tilde{v}}}{\tilde{s}_{\tilde{\tau}}m_{\tau}s_{v}} = 1\,, \qquad v'\frac{m_z|\mathbf{s}|}{\tilde{m}_{\tilde{z}}|\tilde{\mathbf{s}}|} = 1 \quad (14)$$

be valid in a new material space (m_v, m_τ, and m_z) in order to mimic the behavior of light in the virtual space (with anisotropic material properties $\tilde{m}_{\tilde{v}}$, $\tilde{m}_{\tilde{\tau}}$, and $\tilde{m}_{\tilde{z}}$) [3].

Hence, if a virtual free space ($\tilde{m}_{\tilde{v}} = \tilde{m}_{\tilde{\tau}} = \tilde{m}_{\tilde{z}} = 1$) is stretched or compressed, we obtain

$$\varepsilon_v = v'\frac{s_v\tilde{s}_{\tilde{\tau}}}{\tilde{s}_{\tilde{v}}s_{\tau}}\,, \qquad \varepsilon_\tau = \varepsilon_v^{-1}\,, \qquad \mu_z = \frac{|\tilde{\mathbf{s}}|}{v'|\mathbf{s}|} \quad (15)$$

$$(\mathbf{H} = \hat{\mathbf{e}}_z H_z\,,\ \text{TM case})\,,$$

$$\mu_v = v'\frac{s_v\tilde{s}_{\tilde{\tau}}}{\tilde{s}_{\tilde{v}}s_{\tau}}\,, \qquad \mu_\tau = \mu_v^{-1}\,, \qquad \varepsilon_z = \frac{|\tilde{\mathbf{s}}|}{v'|\mathbf{s}|} \quad (16)$$

$$(\mathbf{E} = \hat{\mathbf{e}}_z E_z\,,\ \text{TE case})\,.$$

The identities above define the material transformation laws that can be easily reproduced in noncylindrical, orthogonal, curvilinear coordinates and are valid far beyond their initial cloaking applications [6, 36-40]. Hence, *designing a new anisotropic, continuous material space supporting a required light wave behavior, which is completely equivalent to the behavior of light waves in a virtual free space, is achieved via Eqns* (15) *and* (16).

Therefore, scaling transformations that expand the initially small virtual domain onto a larger material domain are pertinent to imaging or light concentration [10, 34]; by contrast, typical cloaking applications require scaling transforms that shrink the initially larger space to arrange voids that are excluded from the initial virtual domain and are therefore inaccessible to light waves. In both applications, the initial virtual spaces share a common input with the rest of the transformed physical world. Figure 2 shows examples of different scaling transformations.
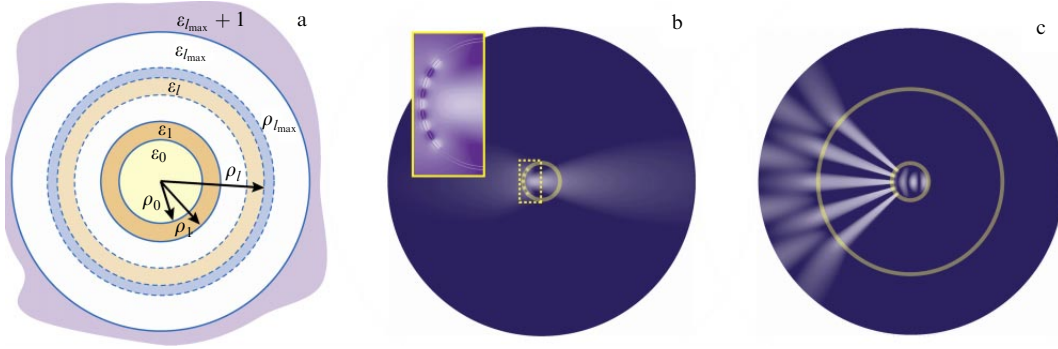
Figure 3. Concentric, cylindrical multilayered hyperlens. (a) Geometry of the layers. Five test sources with subwavelength spacing: (b) free-space radiation (the inset shows zoomed sources), (c) the same sources magnified by the hyperlens.

In FWTO devices based on the scaling transformation approach (e.g., optical cloaks and hyperlenses), a seemingly inevitable drawback of impedance mismatch (and therefore undesired reflection) exists. Indeed, because the simplest linear mapping functions $v(\tilde{v})$ are generally favorable due to their easier material implementations, we have proposed an approach to minimize reflection losses via impedance matching at the input or output boundaries. We demonstrated that comparable performance can be achieved in an optimized, nonmagnetic design of an impedance-matched hyperlens [34]. In parallel, in [41] we proposed using a special type of smooth, high-order transformation in yet another TO device in order to match the impedance at the outer boundary of an optical cloak, hence completely eliminating the detrimental scattering within the limit of geometric optics. In that study, the scattered field in a nonmagnetic, cylindrical cloak with an optimal quadratic transformation was substantially reduced compared to its linear counterpart.

3. TO of multilayer cylindrical devices

Theoretically, FWTO devices with all their fascinating properties can be obtained via 3D optical MMs designed for extreme control over the flow of light on both the nano- and macroscopic scales. However, the realization of 3D TO devices requires the development of advanced fabrication methods for creating complex metal–dielectric composite structures arranged of elements/layers whose dimensions are significantly smaller than the operational wavelength. In addition to the challenging geometries and deeply sub-wavelength features to be manufactured, the quality of the fabricated structures (such as size control and surface roughness) must be carefully optimized to ensure the desired optical performance of TO-device prototypes.

The current techniques of fabrication are conventionally centered on planar technologies, where the fabricated structures are mainly planar or have low aspect ratios. Also, the current fabrication techniques can typically only produce structures with mostly simple, orthogonal 3D geometries and, rarely, beveled 3D structures. However, the fabrication of TO devices requires the capability of making structures with complex geometries and curved interfaces, tapered layers, and layers with gradients in composition and thickness. These requirements are hard to address with conventional fabrication techniques. It is no surprise, then, that the very first attempts at designing and making TO imaging and sensing devices have been focused on TO devices with the simplest

cylindrical symmetries and cylindrical, lamellar metamaterial designs [42].

In Section 3.1, we review an important correction to the design principles of circular, lamellar structures dealing with the effective medium theory of homogenized bilayers. The proposed approach is also used with our modeling tool described in Section 4.2.

3.1 Advanced effective medium theory

In the practice of designing even the simplest cylindrical, engineered metamaterial spaces, a smooth, ideal distribution of the anisotropic material parameters is approximated by just a few elemental materials. Typically, subwavelength-sized bilayers of dispersive and nondispersive elemental materials are arranged to provide the desired effective properties as shown in Fig. 3a, which depicts the concentric, multilayered structure of a cylindrical hyperlens and the resolution from subwavelength-sized sources. In Ref. [43], we showed that the effective material properties of a binary-phase cylindrical structure cannot be adequately approximated by the classical anisotropic effective permittivity of a planar lamellar structure,

$$\varepsilon_{\rho,l}^{-1} = \frac{\varepsilon_l^{-1} t_l + \varepsilon_{l+1}^{-1} t_{l+1}}{t_l + t_{l+1}}, \qquad \varepsilon_{\phi,l} = \frac{\varepsilon_l t_l + \varepsilon_{l+1} t_{l+1}}{t_l + t_{l+1}}, \qquad (17)$$

and that much better performance can be obtained from the approximations

$$\varepsilon_{\rho,l}^{-1} \ln \frac{\rho_{l+2}}{\rho_l} = \varepsilon_l^{-1} \ln \frac{\rho_{l+1}}{\rho_l} + \varepsilon_{l+1}^{-1} \ln \frac{\rho_{l+2}}{\rho_{l+1}},$$

$$\varepsilon_{\phi,l} \ln \frac{\rho_{l+2}}{\rho_l} = \varepsilon_l \ln \frac{\rho_{l+1}}{\rho_l} + \varepsilon_{l+1} \ln \frac{\rho_{l+2}}{\rho_{l+1}}, \qquad (18)$$

where t_l, t_{l+1} and ε_l, ε_{l+1} are the thicknesses and isotropic dielectric functions of two adjacent layers with the respective radii ρ_l, ρ_{l+1} and ρ_{l+1}, ρ_{l+2} ($t_l = \rho_{l+1} - \rho_l$ and $t_{l+1} = \rho_{l+2} - \rho_{l+1}$). Because $\ln(1 + x) \approx x + O(x^2)$, for very thin layers, Eqn (18) becomes the familiar expressions for the effective permittivity of a planar, lamellar structure (17).

It was essential to validate which of the two effective medium formulations, (18) or (17), provides better performance for a given binary, circular hyperlens with the same thickness. It appeared that within our test range, a lens with uniformly spaced layers (lens A) always gave worse resolution than a lens with a nonuniform spacing (lens B) if the same number of layers and the same total thickness of the lens was
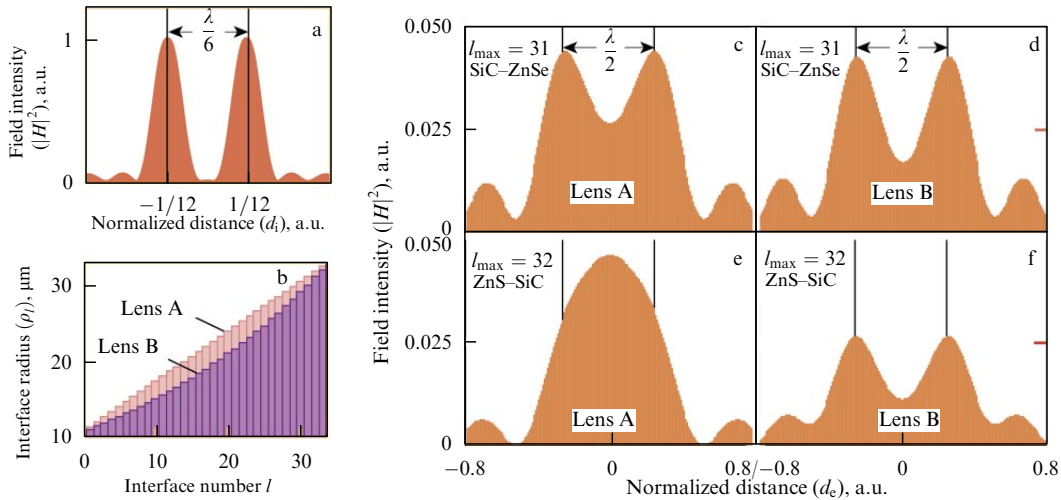
Figure 4. (a) Input magnetic field intensity at ρ_0 used for all tests. (b) Comparison of the nonuniform distribution of ρ_l obtained from Eqn (9) and the uniform distribution; $l_{max} = 34$ has been taken for this example. (c–f) Output image from lens A vs. the image from lens B obtained at the output boundary. (c) Lens A with 31 layers; the initial order of layers is SiC–ZnSe. (e) Lens A with 32 layers; the initial order of layers is ZnSe–SiC. (d) and (f) Same as (c) and (e), but for lens B.

preserved. Figure 4 illustrates a representative example of this observation, where Fig. 4a depicts the input magnetic field intensity at the inner radius ρ_0 used for all tests. Figure 4b compares the nonuniform distribution of ρ_l with the uniform distribution, and $l_{max} = 34$ has been taken for this example. Figures 4c, e indicate that the uniformly spaced lens (lens A) cannot resolve the test image for $l_{max} = 31, 32$, taken with the best-performing order of elementary layers (SiC–ZnSe, for $l_{max} = 31$, and ZnSe–SiC for $l_{max} = 32$). For comparison, Fig. 4d and Fig. 4f show that lens B with the same number of layers already works quite well, even for such small numbers of layers.

In the last few years, some nonlocal corrections to the quasistatic homogenization technique of anisotropic materials have been applied to lamellar structures with subwavelength-thick layers (see, e.g., [44]), and near-term work could include the incorporation of nonlocal adjustments for a cylindrical system. The planar hyperlens described in Section 2.4 and other hyperlens versions described in [10, 32, 34, 42, 45] enable the magnification of low subwavelength images up to sizes that are above the diffraction limit, and thus could offer detection with conventional optics.

Clearly, inverting the process of imaging with a magnifying hyperlens (i.e., by sending light from the other side of the hyperlens) is an efficient way to concentrate light to a spot much smaller than the wavelength. This approach, which could be of particular importance for micro-lenslets, enables the 'collection' of light from wider directions in space and highly localizing that light in nm-scale volumes.

3.2 Omnidirectional light absorbers
Among the possible variations of light concentrators, the TO-based optical black hole — an omnidirectional light absorber — is of particular interest [11, 46, 47] due to the advantage that TO black holes can be realized in a purely dielectric design, without resorting to metal elements and their inherent loss due to free carrier absorption. The approach does not rely on any resonance or anisotropy and leads to high omnidirectional absorption within a broad bandwidth. In particular, one of the key challenges in sunlight harvesting is the diffuse

and low-density nature of solar energy. A solar collector should be optimally oriented towards the sun to transform the maximum amount of light; normally it cannot collect light scattered from the ground or other objects in complex urban or natural environments. One approach to address this problem, especially in low-power light-harvesting devices, is to use omnidirectional light concentrators. Such devices could be critical for mobile or stationary low-power supply systems and, more than ever, in independent 'drop-and-forget' unattended sensing and communication applications.

Figure 5a depicts a beam completely captured by a light absorber and another beam propagating below the device. Figure 5b, c show two designs for a light concentrator; one is a spherical design and the other is a cylindrical design. The center core of the spherical or cylindrical designs is made of a good optical absorber, while the outer cladding is an all-dielectric design with a radial gradient in the refractive index. This directly translates to a radial gradient in the composition of the cladding material. Therefore, the devices require a nonplanar geometry with a graded material system. The fabrication of such structures clearly requires nonplanar technologies with fine control over the composition of the structural elements. This level of control is extremely difficult to accomplish even with the best conventional planar fabrication technologies. Therefore, a nonstandard fabrication technology complementing the existing conventional techniques is a critical element in realizing TO devices. The fabrication of TO devices necessitates the use of dedicated equipment and special processing techniques that can offer the required capabilities with good process control as well as the essential flexibility for research.

Here, to illustrate the differences between the FWTO and SCTO concepts, we outline the semiclassical theory of the omnidirectional light concentrator. The derivation does not directly employ the invariance of Maxwell's equations and is also somewhat different from our recent discussion in [46].

The Fermat principle states that light always minimizes the optical path length, i.e., light propagates from point A to point B using the trajectory $\gamma(A, B)$ that minimizes the integral $F(\gamma) = \int_{\gamma(A,B)} n \, d\gamma$. We take a circular cylinder with a
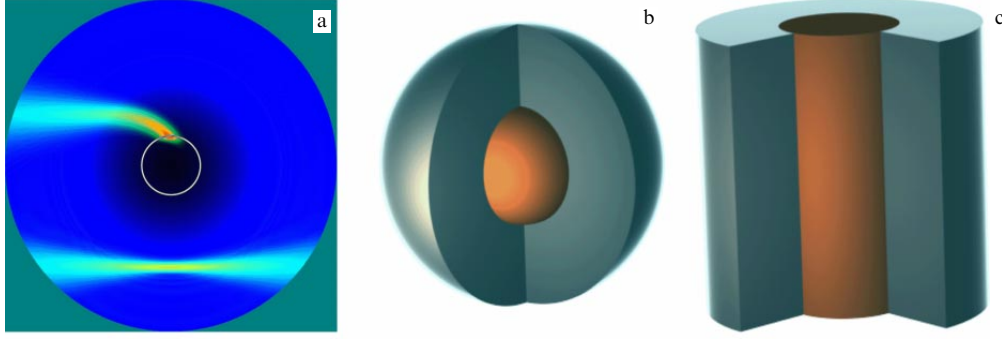
Figure 5. (a) A simulated light beam completely captured by the light absorber. The other beam propagares below, missing the device. (b, c) Schematic cross-section of light concentrators using all-dielectric designs. The center core is made of a strong light absorber, and the outer cladding is made of a dielectric material with a graded refractive index: (b) spherical design and (c) cylindrical design.

radius-dependent refractive index $n(r)$ and write the trajectories of light in cylindrical coordinates as $r\hat{\mathbf{e}}_r + \phi(r)\hat{\mathbf{e}}_\phi$ (with $x = r\cos\phi$ and $y = r\sin\phi$). In this case, the line element ds is given by $(1 + r^2\phi'^2)^{1/2}\,dr$ (with $\phi' = d\phi/dr$), and the length of the optical path is given by

$$F(r, \phi, \phi') = \int_{r_A}^{r_B} f\,dr, \quad f = n(r)\sqrt{1 + r^2\phi'^\phi}. \tag{19}$$

We now write the necessary condition for the shortest optical path by setting the derivative of the above functional to zero,

$$\frac{\partial F}{\partial \phi} = \int_{r_A}^{r_B} \frac{\partial f}{\partial \phi}\,dr = 0. \tag{20}$$

The identity holds for any r_A and r_B; because all the functions are continuous, this implies that the integrand also vanishes:

$$0 = \frac{\partial f}{\partial \phi} = \frac{d}{dr}\left[\frac{\partial f}{\partial \phi'}\right] = \frac{d}{dr}\left[\frac{n(r)r^2\phi'}{\sqrt{1 + r^2\phi'^2}}\right]. \tag{21}$$

Equation (21) requires that $\partial f/\partial \phi' = c_0$, where c_0 is a constant defined by the direction and position of the incident light beam,

$$c_0 = \frac{n(r)r^2\phi'}{\sqrt{1 + r^2\phi'^2}}. \tag{22}$$

We now recall that (as for any curve in polar coordinates) the angle φ between the ray direction and the radius vector at any point (r, ϕ) is defined by $\varphi = \tan^{-1}(r\phi')$. Then (22) can be rewritten as

$$c_0 = n(r)r\sin\varphi, \tag{23}$$

which gives *Snell's law for any point inside a cylindrical lens with a radial gradient of n*.

    We assume that a beam coming from the host medium is parallel to the x axis ($\varphi_0 = \phi_0$). Then c_0 is defined by the initial vertical position of the acceptance point $y_0 = r_s\sin\phi_0$ and the dielectric permittivity of the homogeneous host medium $\varepsilon_s = n^2(r_s)$,

$$c_0^2 = \varepsilon_s y_0^2. \tag{24}$$

Then Eqn (22) can be rewritten as

$$\phi' = \left(r\sqrt{\frac{\varepsilon}{\varepsilon_s}\frac{r^2}{y_0^2} - 1}\right)^{-1}. \tag{25}$$

If the radial dependence of the dielectric permittivity is given by $\varepsilon(r) = \varepsilon_s(r_s/r)^p$, we finally obtain the trajectories

$$\phi(\tilde{r}) = \phi_0 - \sin\phi_0\int_1^{\tilde{r}} \tilde{r}^{-1}(\tilde{r}^{2-p} - \sin^2\phi_0)^{-1/2}\,d\tilde{r}, \tag{26}$$

where $\tilde{r} = r/r_s$. For $p = 2$, this takes the simple form $\phi = \phi_0 - \ln\tilde{r}\tan\phi_0$, or

$$r(\phi) = r_s\exp\left[\cot\phi_0\,(\phi_0 - \phi)\right]. \tag{27}$$

In the general case $p \neq 2$, we change the integration variable as $\xi = \tilde{r}^{(2-p)/2}$, with the result

$$\phi(\xi) = \phi_0 - \frac{2}{2-p}\sin\phi_0\int_1^{\xi} \frac{d\xi}{\xi\sqrt{\xi^2 - \sin^2\phi_0}}. \tag{28}$$

Calculating the integral as

$$\int \frac{dx}{x\sqrt{x^2 - a^2}} = |a|^{-1}\tan^{-1}\frac{|a|}{\sqrt{x^2 - a^2}},$$

we then obtain

$$\phi(\xi) = \phi_p + \frac{2}{2-p}\,\text{sgn}\,(\sin\phi_0)$$
$$\times \tan^{-1}\left(|\sin\phi_0|(\xi^2 - \sin^2\phi_0)^{-1/2}\right),$$

where

$$\phi_p = \phi_0\left(1 - \frac{2}{2-p}\,\text{sgn}\,(\sin\phi_0)\right).$$

Hence,

$$r(\phi) = r_s\left(\sin^2\phi_0\csc^2\left[\frac{2-p}{2}(\phi_p - \phi)\right]\right)^{1/(2-p)}. \tag{29}$$

A simulated example of such an optical black hole is shown in Fig. 6a. As depicted in Fig. 6a, b, any ray of light is captured by the outer shell and absorbed in the central core of the
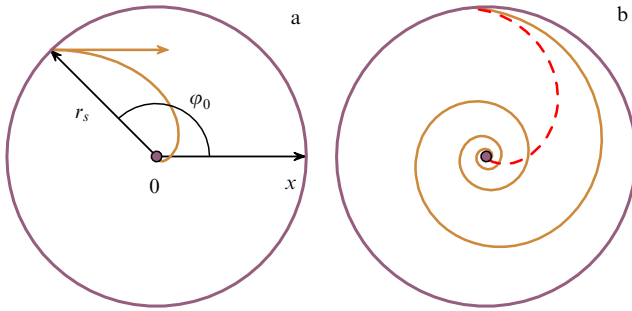
Figure 6. (a) Beam incident on the device at $\phi_0 = 3\pi/4$; the light trace is shown for $p = 2$. (b) Comparison of traces for $\phi_0 = 0.55\pi$, $p = 2$ (orange line) and $p = 3$ (red line).
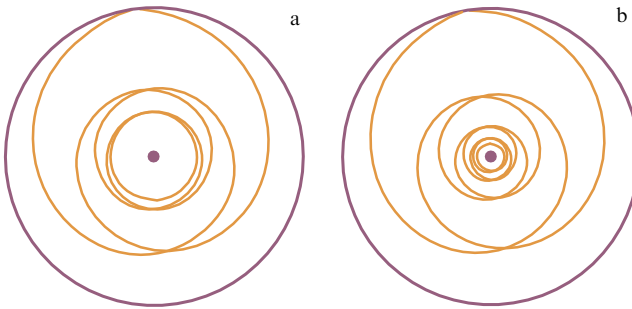

Figure 7. The trace of the light beam incident on the device at $\phi_0 = 0.55\pi$ (a) $p = 1.98$, the beam makes about 10 turns; (b) $p = 1.99$, the beam makes 20 turns.

optical black hole device. By contrast, a metamaterial space with $p < 2$ cannot capture light, as shown in Figs 7a, b, and the trace of the light beam incident on the device at $\phi_0 = 0.55\pi$ makes 10 turns (Fig. 7a, $p = 1.98$) or 20 turns (Fig. 7b, $p = 1.99$) before leaving the light trap.

4. Free access to the results and methods of studying TO devices

Knowledge transfer should be an important component of research. Below, we describe our activities in this direction. In addition to conventional publications, conference talks, and seminars, dissemination of knowledge to a broader community of scientists, engineers, educators, students, and the general public is arranged via the nanoHUB.org web site supported by the Network for Computational Nanotechnology headquartered at Purdue University. The knowledge gained in ongoing metamaterial research is translated into educational resources: tutorials, learning modules, complete courses, and simulation tools. These last are not only an interactive supplement to traditional courses but also a useful research tool. All software is freely available to registered users and is provided with a convenient graphic web interface.

4.1 Nanophotonics tools in the nanoHUB environment
The substantial advances in active optical metamaterials [48, 49], scalable computational electromagnetics, Internet-based infrastructure, and parallel computers already enable us to boost the progress in nanophotonics through cloud computing services. Today, nanoHUB nanophotonics tools support true in-the-cloud execution, giving an offsite, installation-free, hardware-independent service. The free tools are accessed via the Internet: the required front-end client is

only a standard browser with standard universal network access. The tools are supported by video tutorials, and hence very minimal initial skills are required for their efficient use. For example, a videotaped course of lectures by one of the authors (VMS) entitled "Nanophotonics and Metamaterials" has been viewed by about 20,000 viewers from all over the world.

Our overall objective is to develop a series of nanophotonics software tools combining intuitive, easy-to-use, standards-based, cross-platform user interfaces with transparent and dynamic access to live and background-running sessions and efficient, near-real-time execution. Our specific aim is to make the tools progressively more uniform in terms of the user interface and common pre- and post-processing services and thus give users an immediate insight into how each of the tools could be used to enter the problem geometry and other parameters, or to present the simulation results.

We have already developed an initial series of two design tools (Hyperlens Layer Designer and Hyperlens Design Solver) for a transformation optics device — a magnifying hyperlens — and four other UI-cohesive nanophotonics tools (PhotonicsDB, PhotonicsRT, PhotonicsSHA-2D, and PhotonicsCL). All these tools are already staged at nano-HUB, providing a set of free cloud-computing services, such as approximating and comparing the frequency dispersive optical properties of various materials (PhotonicsDB), designing planar nanostructured lamellar photonic crystals and nonreflecting coatings (PhotonicsRT), user-customized cascaded photonic or plasmonic 2D metamaterials (PhotonicsSHA-2D), user-customized cylindrical transformation-optics lenses (PhotonicsCL), and cylindrical hyperlenses (Hyperlens Layer Designer and Hyperlens Design Solver). The selected tools mentioned here have assisted more than 880 users who have run 12,290 jobs to date.

In this section, we review our recent progress pertinent to the development and deployment of this easy-to-use, multi-faceted, on-line research environment for the nanophotonics research community. In particular, we show representative examples of two online software tools addressing a growing need for efficient numerical simulations in the area of transformation optics.

The selected tools, which are freely available at nano-HUB.org, cover the design and simulation of transformation-optics devices, a cylindrical lamellar hyperlens and an optical black hole already discussed in Section 4. The tools deliver a cloud-computing service, offering off-site simulations done through standard web browsers, with no need for either any powerful computational hardware or any additional software installations.

4.2 Hyperlens designer
A hyperlens, already discussed in Section 3, is a magnifying optical lens capable of overcoming the diffraction limit by taking advantage of a hyperbolic dispersion relationship inside a specifically designed plasmonic structure [45, 50–52]. The hyperlens design toolset consists of two separate tools: Hyperlens Layer Designer [53] and Hyperlens Design Solver [54].

The Hyperlens Layer Designer allows users to quickly and easily create hyperlens designs and save them for later use in the Hyperlens Design Solver. It allows users to upload designs, make a new design, or select from several pre-existing designs. The Hyperlens Design Solver is intended to be used in conjunction with the Hyperlens Layer Designer to
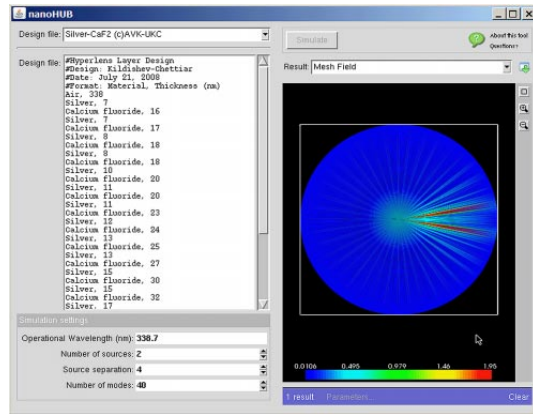
Figure 8. User interface of Hyperlens Design Solver.

assist with the design and simulation of a hyperlens. It simulates the performance of the design and outputs several plots of the resulting field intensities. By using these two tools, users can experiment with different designs and compare their performance to find the optimal layered structure before beginning fabrication.

The hyperlens that can be designed and simulated by the Hyperlens Layer Designer is a circular cylindrical, multi-layered structure comprising a number of cylindrical inter-faces of lamellar media, as shown in Fig. 3a. The axes of the concentric cylindrical surfaces are assumed to coincide with the z axis of a common cylindrical coordinate system. The point sources for evaluating performance are placed inside the innermost cylinder. The number of sources and the distance between the sources can be adjusted in the tool. Figure 8 shows the user interface of the Hyperlens Design Solver. In the figure, the hyperlens design consists of 35 alternating cylindrical silver and calcium fluoride layers with incrementally increasing subwavelength thicknesses, as shown in the left panel. Two point sources inside the hyperlens with a quarter-wavelength separation are also set in the input panel. The calculated field intensity distribution of the hyperlens is shown in the right panel, which reveals that the two sources are clearly resolved, even though the distance between them is below the diffraction limit. It can also be observed that the scale of the image at the outer surface of the hyperlens is substantially larger than the source distance. The output image scale can be larger than the wavelength; thus further optical processing at the outer surface is possible. A comprehensive analysis of different designs using this tool has been performed in [43].

4.3 PhotonicsCL

PhotonicsCL [55] is used for designing and simulating the circular cylindrical, multilayered and graded index structures described in the preceding section (see Fig. 8). However, PhotonicsCL is more powerful than the Hyperlens Layer Designer. First, the designed, multilayered, cylindrical struc-ture can serve as a piecewise-constant approximation for a variety of ideal optical devices with continuous distributions of material constants, e.g., Eaton lenses, Luneburg lenses, and optical 'black hole' devices (omnidirectional light concentrators and absorbers [47, 56, 57]). Also, the direct simulation of an ideal optical black hole is available. Second, the tool allows for different types of light sources, including plane-wave sources and multiple Gaussian-beam sources. It also has a link to the PhotonicsDB material database and can use all the database materials, as well as user-specified materials, in the design.

Figure 9a shows the user interface of PhotonicsCL while the tool is simulating a multilayered optical black hole device with Gaussian-beam illumination from the left. The simu-lated field intensity inside the device is shown in Fig. 9b. It reveals that the light beam bends towards the center and is totally absorbed by the device core.

5. Summary and future work

The fundamentals of transformation optics with metamater-ials and novel, critical TO devices were briefly reviewed in Sections 2 and 3. The proposed light concentrating devices, including a flat hyperlens and an omnidirectional absorber, can be used for innovative sensing, optical nanofabrication techniques, nanoscale-resolution imaging through add-on tools for standard microscopes, and mobile and stationary photovoltaic low-power supply systems for unattended sensing and communication applications.

Although the theoretical aspects of the TO devices and the methods for designing the desired metamaterial spaces for light are also important, the major challenges are clustered in the necessary nanofabrication capabilities and the limited choice of elemental plasmonic materials.

One challenge with employing TO devices using plasmo-nic components is to overcome the large losses in the metal constituent materials. While metals work well for low incident light frequencies, they begin to suffer from high interband transition losses as the incident light approaches the tele-communication and visible frequencies. Currently, the most common solution to the problem of losses is to use gain media as host materials, such that losses inherent in the plasmonic structures can be compensated by the gain in the host. It was pointed out recently that energy can be transferred from a gain material to surface plasmon polaritons or to plasmons in metal nanostructures using stimulated emission. The idea to use gain media to offset losses in *propagating* surface plasmon polaritons (SPPs) was considered in [58–60] and in *localized* surface plasmons (LSPs) in [61]. Using amplification for balancing losses in negative-index materials (NIMs) was first proposed in [12]. This approach has already shown some promising first experimental results [62–66], which include the demonstration of the world's smallest laser accomplished through a Cornell – Norfolk State – Purdue collaboration [67], and has culminated in the most recent experimental demonstration of an active NIM performed by our group at Purdue [48]. Another complementary approach is based on using TO devices with new, nonmetallic plasmonic components with lower losses, such as highly doped trans-parent conducting oxides and intermetallics; this approach is currently being pursued by the Boltasseva group at Purdue [68, 69].

Our research is tightly linked to its education and technology transfer initiatives. The nanofabrication and advanced modeling approaches developed in our group are extremely valuable for training students in state-of-the-art nanotechnologies, nanophotonics, material science, large-scale numerical simulations, and cloud-computing technolo-gies. In this paper, we introduced nanoHUB.org, a powerful scientific and educational cloud service and cyber-infrastruc-ture for the nanotechnology community. We reviewed a series of our nanophotonics tools [53–55, 70–72] that are staged at nanoHUB and are free to use.
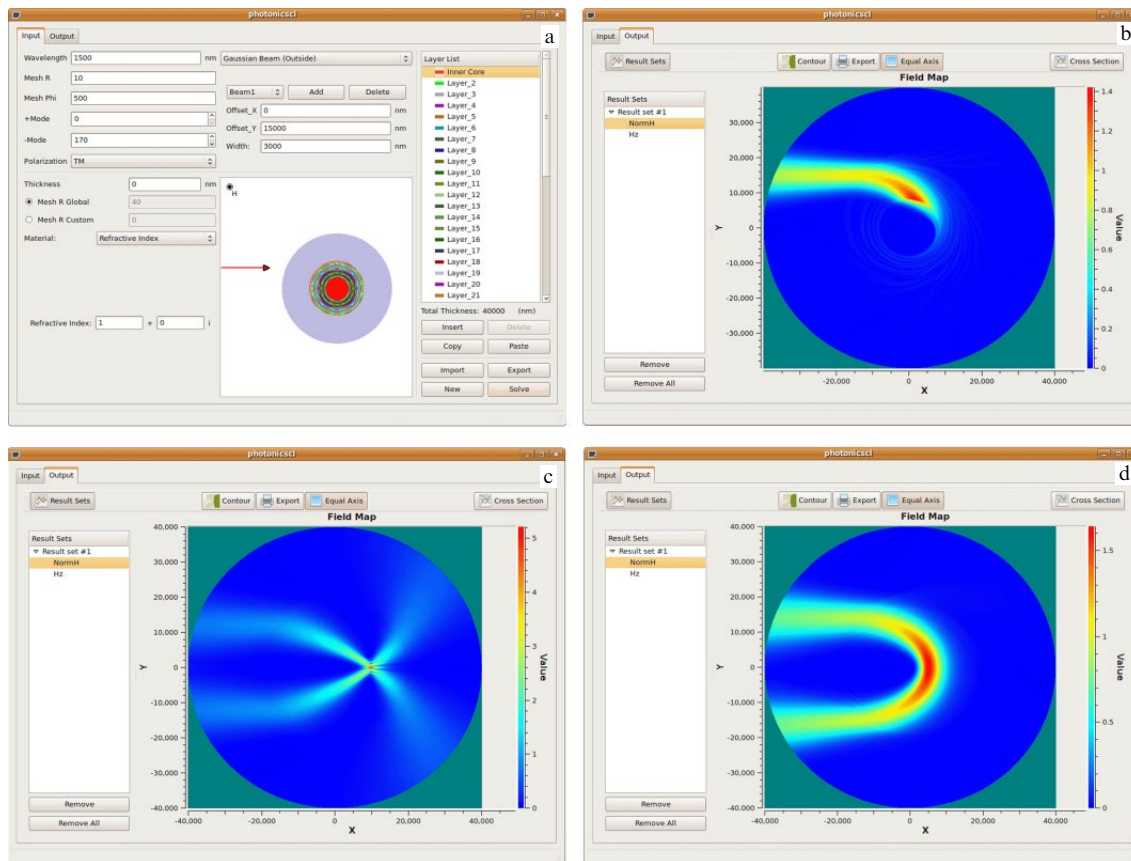
Figure 9. User interface of PhotonicsCL: input panel (a) and output panel with a simulated lamellar light absorber (b). (c, d) Output examples with simulated Luneberg (c) and Eaton (d) lenses.

We fully believe that our current and future research in the area of material science and advanced design and fabrication techniques for developing active and low-loss metamaterial-based TO devices, including the theoretical cloud-based simulation and modeling tools, will be highly instrumental for achieving the desired precise manipulation of light in future information-processing devices, sensing for medicinal and bio-medical areas, unattended or mobile low-power supply systems based on sunlight harvesting, and other applications.

References

1. Shalaev V M et al. *Opt. Lett.* **30** 3356 (2005)
2. Shalaev V M *Nature Photon.* **1** 41 (2007)
3. Pendry J B, Schurig D, Smith D R *Science* **312** 1780 (2006)
4. Leonhardt U *Science* **312** 1777 (2006)
5. Shalaev V M *Science* **322** 384 (2008)
6. Dolin L S *Izv. Vyssh. Uchebn. Zaved. Radiofiz.* **4** 964 (1961)
7. Leonhardt U *New J. Phys.* **8** 118 (2006)
8. Kildishev A V, Cai W, Chettiar U K, Shalaev V M *New J. Phys.* **10** 115029 (2008)
9. Cai W, Chettiar U K, Kildishev A V, Shalaev V M *Nature Photon.* **1** 224 (2007)
10. Kildishev A V, Shalaev V M *Opt. Lett.* **33** 43 (2008)
11. Narimanov E E, Kildishev A V *Appl. Phys. Lett.* **95** 041106 (2009)
12. Ramakrishna S A, Pendry J B *Phys. Rev. B* **67** 201101 (2003)
13. Leonhardt U, Philbin T G *New J. Phys.* **8** 247 (2006)
14. Schurig D et al. *Science* **314** 977 (2006)
15. Schurig D, Pendry J B, Smith D R *Opt. Express* **14** 9794 (2006)
16. Shyroki D M *IEEE Microwave Wirel. Compon. Lett.* **16** 576 (2006)
17. Schurig D, Pendry J B, Smith D R *Opt. Express* **15** 14772 (2007)
18. Rahm M et al. *Phys. Rev. Lett.* **100** 063903 (2008)
19. Rahm M et al. *Photon. Nanostruct. Fundament. Appl.* **6** 87 (2008)
20. Zhang P, Jin Y, He S *Opt. Express* **16** 3161 (2008)
21. Narimanov E E, Shalaev V M *Nature* **447** 266 (2007)
22. Lass H *Vector and Tensor Analysis* (New York: McGraw-Hill, 1950)
23. Veselago V G *Usp. Fiz. Nauk* **92** 517 (1967) [*Sov. Phys. Usp.* **10** 509 (1968)]
24. Veselago V G *Usp. Fiz. Nauk* **172** 1215 (2002) [*Phys. Usp.* **45** 1097 (2002)]
25. Veselago V G *Usp. Fiz. Nauk* **173** 790 (2003) [*Phys. Usp.* **46** 764 (2003)]
26. Veselago V G *Usp. Fiz. Nauk* **179** 689 (2009) [*Phys. Usp.* **52** 649 (2009)]; Veselago V G, Shchavlev V V *Usp. Fiz. Nauk* **180** 331 (2010) [*Phys. Usp.* **53** 317 (2010)]
27. Pendry J B *Phys. Rev. Lett.* **85** 3966 (2000)
28. Lagarkov A N et al. *Usp. Fiz. Nauk* **179** 1018 (2009) [*Phys. Usp.* **52** 959 (2009)]
29. Veselago V G, in *Advances in Electromagnetics of Complex Media and Metamaterials* (NATO Sci. Ser., Ser. II, Vol. 89, Eds S Zouhdi, A Sihvola, M A Arsalane) (Dordrecht: Kluwer Acad. Publ., 2002) p. 83
30. Ramakrishna S A et al. *J. Mod. Opt.* **50** 1419 (2003)
31. Taubner T et al. *Science* **313** 1595 (2006)
32. Jacob Z, Alekseyev L V, Narimanov E *Opt. Express* **14** 8247 (2006)

33. Jacob Z, Alekseyev L V, Narimanov E *J. Opt. Soc. Am. A* **24** A52 (2007)
34. Kildishev A V, Narimanov E E *Opt. Lett.* **32** 3432 (2007)
35. Rahm M et al. *Photon Nanostruct.* **6** 87 (2008)
36. Greenleaf A et al. *Opt. Express* **15** 12717 (2007)
37. Jacob Z, Narimanov E E *Opt. Express* **16** 4597 (2008)
38. Kwon D-H, Werner D H *Appl. Phys. Lett.* **92** 113502 (2008)
39. Weder R *J. Phys. A Math. Theor.* **41** 065207 (2008)
40. Zharova N A, Shadrivov I V, Kivshar Yu S *Opt. Express* **16** 4615 (2008)
41. Cai W, Chettiar U K, Kildishev A V, Shalaev V M, Milton G W *Appl. Phys. Lett.* **91** 111105 (2007)
42. Zhang X, Liu Z *Nature Mater.* **7** 435 (2008)
43. Kildishev A V, Chettiar U K, Jacob Z, Shalaev V M, Narimanov E E *Appl. Phys. Lett.* **94** 071102 (2009)
44. Avrutsky I *J. Opt. Soc. Am. A* **20** 548 (2003)
45. Liu Z et al. *Science* **315** 1686 (2007)
46. Kildishev A V, Prokopeva L J, Narimanov E E *Opt. Express* **18** 16646 (2010)
47. Genov D A, Zhang S, Zhang X *Nature Phys.* **5** 687 (2009)
48. Xiao S et al. *Nature* **466** 735 (2010)
49. Wuestner S et al. *Phys. Rev. Lett.* **105** 127401 (2010)
50. Ni X, Jacob Z, Kildishev A, Shalaev V, Narimanov E E "A tool for designing realizable hyperlenses", in *Conf. on Lasers and Electro-Optics/Intern. Quantum Electronics Conf., OSA Technical Digest* (*CD*) (Optical Society of America, 2009), paper JWA110
51. Fang N et al. *Science* **308** 534 (2005)
52. Smolyaninov I I, Hung Y-J, Davis C C *Science* **315** 1699 (2007)
53. Swanson M, Kildishev A V, Ni X "Hyperlens layer designer" (2008), DOI: 10254/nanohub-r4703.1
54. Swanson M, Ni X, Jacob Z, Kildishev A V "Hyperlens design solver" (2008), DOI: 10254/nanohub-r4770.4
55. Ni X, Gu F, Prokopeva L, Kildishev A V "PhotonicsCL: Photonic cylindrical multilayer lenses" (2010), DOI: 10254/nanohub-r9914.1
56. Kildishev A V et al. "Optical black hole: design and performance", in *Quantum Electronics and Laser Science Conf., OSA Technical Digest* (*CD*) (Optical Society of America, 2010), paper JWA10
57. Cheng Q et al. *New J. Phys.* **12** 063006 (2010)
58. Avrutsky I *Phys. Rev. B* **70** 155416 (2004)
59. Bergman D J, Stockman M I *Phys. Rev. Lett.* **90** 027402 (2003)
60. Nezhad M, Tetz K, Fainman Y *Opt. Express* **12** 4072 (2004)
61. Lawandy N M *Appl. Phys. Lett.* **85** 5040 (2004)
62. Noginov M A et al. *Opt. Express* **16** 1385 (2008)
63. Noginov M A et al. *Appl. Phys. B* **86** 455 (2007)
64. Noginov M A et al. *Opt. Lett.* **31** 3022 (2006)
65. Noginov M A et al. *Phys. Rev. Lett.* **101** 226806 (2008)
66. Seidel J, Grafström S, Eng L *Phys. Rev. Lett.* **94** 177401 (2005)
67. Noginov M A et al. *Nature* **460** 1110 (2009)
68. Naik G V, Boltasseva A *Phys. Status Solidi Rapid Res. Lett.* **4** 295 (2010)
69. West P R et al. *Laser Photon. Rev.* **4** 795 (2010)
70. Ni X, Liu Z, Kildishev A V "PhotonicsDB: Optical constants" (2007), DOI: 10254/nanohub-r3692.10
71. Ishii S, Chettiar U K, Ni X, Kildishev A V "PhotonicsRT: Wave propagation in multilayer structures" (2008), DOI: 10254/nanohub-r5968.14
72. Ni X et al. "PhotonicsSHA-2D: Modeling of single-period multilayer optical gratings and metamaterials" (2009), DOI: 10254/nanohub-r6977.9